Response Analysis and Comparison of a Spar Type and a Land-based Wind Turbines under Blade Pitch Controller Faults

M. Etemaddar [a,b], M. Blanke [b,c], Z. Gao [a,b], T. Moan [a,b]
a. Department of Marine Technology, Norwegian University of Science and Technology (NTNU)
b. Center of Ship and Ocean Structures (CeSOS) , Norwegian University of Science and Technology (NTNU)
c. Automation and Control Group, Department of Electrical Engineering, Technical University of Denmark (DTU)

Abstract
This paper analyses the effects of three pitch controller faults on the responses of a land-based and a spar-type floating wind turbine. These faults include: blade pitch actuator stuck, blade pitch sensor fixed value and bias faults. The faults are modeled in the controller dynamic link library and short-term extreme response and fatigue damage analysis are carried out using the simulation tool HAWC2. Statistical investigations are carried out through the six 1-hour stochastic samples for each load case. Effects of faults on the responses at different wind speeds and fault amplitudes are investigated through the response sensitivity analysis. Severity of individual faults is categorized through the extreme values and fatigue damage. Based on the magnitude of the effect of faults on the extreme values and fatigue damage, structural members were sorted. The pitch sensor fixed value fault is found to be the most severe fault case and the shaft to be the structural member at highest risk. Comparison between the floating and a land-based wind turbines showing that faults cause the bigger damage to the tower and yaw bearing of the land-based and bigger damage to the shaft for the floating wind turbine.

Keywords
Spar Wind Turbine, Land based, Offshore, OC3-Hywin, Pitch Actuator Fault, Pitch Sensor Fault, Pitch Controller Fault, Response Characteristics, Extreme Response, Fatigue Damage

Abbreviations

LWT	Land-based Wind Turbine	BEM	Blade Element Momentum Method
FWT	Floating Wind Turbine	DLL	Dynamic Link Library
PAST	Pitch Actuator Stuck Fault	BR	Blade Root
PSBF	Pitch Sensor Bias Fault	TB	Tower Bottom
PSFV	Pith Sensor Fixed Value Fault	YB	Yaw Bearing
TTF	Time to Fault	SB	Shaft Bearing

Introduction

Operation and Maintenance (O&M) costs of offshore wind turbines are higher than for land-based wind turbines (LWT). The main reason for this is that, offshore wind turbines are located at remote sites with harsh environmental conditions, and there is a limited site access and operational weather window. This also increases the demand for high reliability and low operational costs. Recent studies on developments of O&M plans for offshore wind farms show that the cost for maintenance is about 25 to 30% of energy generation costs [1-3].

There are two main strategies for O&M of wind turbines: corrective maintenance and preventive maintenance. Preventive maintenance can be scheduled or condition-based. The schedule-based O&M strategy seems to be too expensive for offshore wind turbines because some components will be replaced before their actual end of life, and this also increases the logistics and transportation costs. Therefore, condition-based O&M with the help of condition monitoring systems is more attractive for offshore turbines. For condition-based maintenance it is possible to evaluate the health of the system by analyzing data available from existing supervision, control and data acquisition (SCADA). Condition-based maintenance is useful for components which have wear as the primary cause of failure.

Several wind turbine fault cases were simulated in the CONMOW [1] project: rotor mass imbalance and aerodynamic imbalance, as well as blade pitch bearing friction. The aim was to study the resulting output to ascertain the most reliable signal for condition monitoring. The steady-state response of a parked spar-type wind turbine considering baled pitch mechanism fault was studied by Jiang et al. [4]. Results showed that fault with one blade seized often leads to the largest platform roll and yaw angle. The effects of faults on loads and power output of land-based wind turbines have been studied [5-7] for fault detection and isolation as well as structural load analysis purposes. Diagnosis and fault-tolerant control methodologies have been applied in offshore engineering area by Fang, Blanke and Leira (2013) [8], where the safety of structural element is in high concern. Faults in the blade root bending moment strain gauges was simulated for a wind turbine with an individual pitch controller [9]. Active diagnosis was employed to isolate bending moment and pitch sensor faults by Brath, Dalsgaard and Blanke (2011) [10]. Sensor and actuator fault detection for wind turbine system was studied by Wei and Verhaegen [11]. Different types of faults in generator and rotor speed sensors were modeled

and detected by Odgaard and Stoustrup [6, 7]. Different techniques for fault detection based on the SCADA data analysis were described to identify incipient faults in wind turbines[12]. The pitch system data is used to monitor the health of blade pitch system [13]. Generic techniques based on wavelet analysis were shown to have potential to capture multiple types of faults in both mechanical and electrical elements of the turbine, Yang et.al (2010)[14].

Despite its importance for the deployment of floating offshore turbines, there has been sparse research on the effects that particulate faults have on turbine components and therefore on reliability. This study aims to bring some quantitative and qualitative information about the effects of different pitch actuator and controller faults on the loads and structural responses of a floating offshore wind turbine. The OC3-Hywind [15] which is a 5MW variable speed pitch-regulated floating wind turbine (FWT) with spar-type sub-structure and catenary mooring lines is used as a reference in this study. The HAWC2 [16, 17] code, an aero-hydro-servo-elastic code for time domain simulation of offshore wind turbines, is used as the main tool. The code is benchmarked through the IEA code-to-code comparisons [18].

A two-fold objective is pursued in this work: 1) the relationship between the given faults (pitch controller system faults) and the change in the responses of the wind turbine for condition monitoring purposes and 2) structural load analysis under fault conditions including the extreme value and fatigue damage analysis. In this regard three fault cases in the blade pitch controller are modeled and simulated. These fault cases include two pitch sensor encoder faults – pitch sensor fixed value (PSFV) and pitch sensor bias fault (PSBF) – and one pitch actuator fault: pitch actuator stuck (PAST). The responses under fault conditions are compared with the fault-free responses with identical environmental inputs to investigate a measurable response characteristic for fault detection. This is done through the evaluation of change in the first and second order moment of the loads and responses in time domain as well as the spectra of the response in frequency domain. In addition, the effects of faults on the floating offshore and land-based wind turbines are compared to distinguish the probable differences between them and severity of each fault for these two concepts. To achieve the second objective, the structural responses under fault conditions for 6 one-hour stochastic samples are compared with the fault-free responses to determine the change in the extreme values and fatigue damage of the FWT. The short term fatigue damage for each fault case is calculated to show how risky it is to operate the wind turbine under these fault cases.

The paper is organized as follows. Section 2 describes the theoretical background of the problem, including aeroelastic and hydrodynamic theories, controller configuration and fault simulation. Section 3 presents the load case set-up, the effects of faults on the performance parameters through a sensitivity analysis, the effect of faults on the extreme responses and fatigue damage, a comparison between the transient and steady state response under fault conditions and a comparison between the effect of faults on the responses of LWT and FWT. Finally, section 4 presents our conclusions.

Background

Statistical data on wind turbine sub-system failure rates and downtimes per failures are used to evaluate the reliability of wind turbines [19]. Reliability analyses of more than 6000 modern wind turbines and their sub-assemblies in Denmark and Germany over 11 years show that large wind turbines are less reliable than smaller ones. The average failure rate of pitch mechanisms for variable speed pitch-regulated wind turbines is 0.4 per wind turbine per year. The mean time to repair for the pitch controller is around 70 hrs per failure. Ribrant and Bertling [20] show that in Swedish wind power plants 27.5 % of the total failures in components (between 2000-2004) were related to all sensors and pitch systems. In addition, 14.8% of the total downtime was for sensors and blade/pitch system. When sensors and pitch mechanisms cannot be improved, fault diagnosis and fault tolerant control are available to reduce the downtime. A recent study of the detailed wind farm data, has been done by Wilkinson et al. [21], attempts to identify and understand the critical failures and their mechanisms in modern technology wind turbines. Results show that the pitch system has the biggest contribution to both failure rate and downtime of the wind turbine: 15% and 20% respectively.

Prior to developing an efficient condition monitoring system, long-term experience, including measurements during situations with faults and failures, need to be available. Data measurement is also costly and there is limited access to such data due to the confidentiality of industrial projects. Since it is too difficult and expensive to apply fault situations on full-scale wind turbines, simulation

seems to be a helpful approach to determine the relationship between the faults and several measurable parameters.

Theory

Environmental Loads

Wind and waves are two main environmental stochastic load sources for offshore wind turbines. The wind speed kinetic energy distribution in the frequency domain, from a long-term perspective, is defined by the Van der Hoven spectrum [22]. A typical wind spectrum, independent of the site, exhibits two peaks, approximately 0.01 cycles/hour (4-day cycles) and 50 cycles/hour (app. 1 min). The low-frequency side of the spectrum corresponds to the geostrophic winds, while the high-frequency part of the spectrum represents the turbulence associated with the local winds. The concentration of energy around two clearly separated frequencies allows the wind speed signal u, in a short term, to be split into two components: mean wind speed and turbulent wind speed. The Mann turbulence model is used to generate a full 3D turbulent wind filed with correlation between the turbulence in the three directions. The hydrodynamic loads are induced by waves which are irregular and stochastic. The irregular wave is a superposition of regular waves with different amplitudes, frequencies and phases. The contribution of each wave component in the total wave energy is formulated by wave spectra. The sea state is defined by significant wave height H_s and peak spectral period T_p.

To carry out the realistic load analysis for offshore structures, it is important to consider the correlation between the environmental loads. This requires a joint probabilistic model of mean wind speed U_m, H_s and T_p [23]. If the wind speed is chosen as the primary parameter, the joint probability density function will be,

$$f_{U_m H_s T_p}(u,h,t) = f_{U_m}(u) f_{H_s|U_m}(h|u) f_{T_p|H_s U_m}(t|h,u) \quad (1)$$

The environmental data at the Statfjord site [23] are used for this study. The wind environmental data are available for other areas, see Vincent et.al (2012) [24] and references therein.

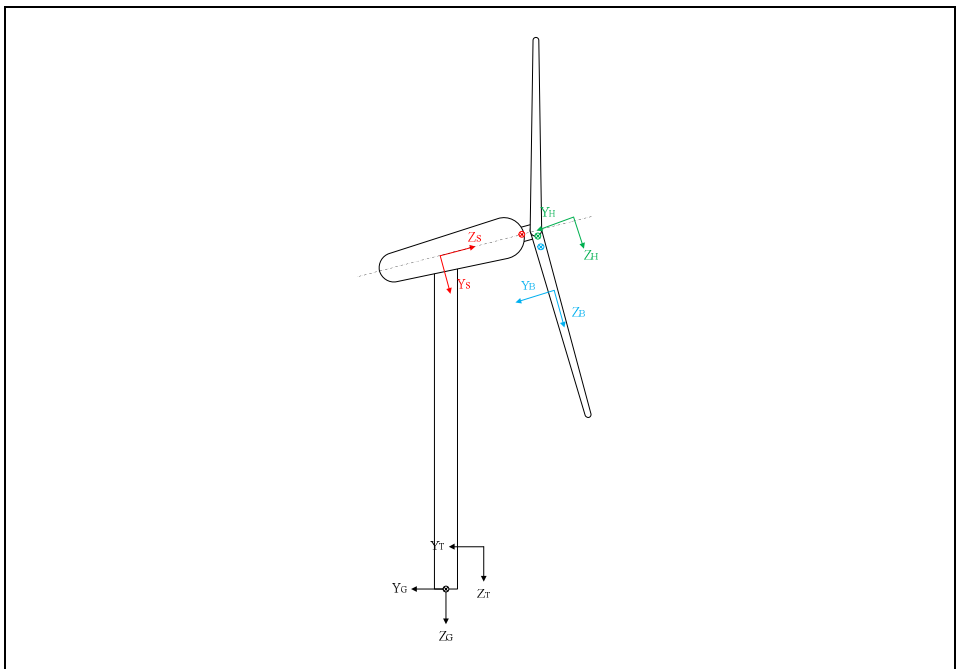

Figure 1. Orientation of local coordinate systems on main structural members
S: Shaft, **B**: Blade, **H**: Hub, **T**: Tower, **G**: Global

Aeroelastic Model

The structural model in HAWC2 is based on a multi-body formulation with each body modeled as a finite element using a Timoshenko beam formulation. The structure consists of three sub structures:

Tower, Nacelle and rotor (blades) for the land-based wind turbine and in addition the SPAR for the floating wind turbine. Each substructure has its own coordinate system allowing for large rotation of substructures. The orientations of local coordinate systems are shown in Figure 1. There are six degrees of freedom for each element node. For a typical wind turbine the total number of DOFs is approximately 250. The aerodynamic model is based on the modified Blade Element Momentum (BEM) method [25]. Unsteady aerodynamic effects are modeled by Beddoes-Leishman type dynamic stall model.

Hydrodynamic Model

The hydrodynamic loads in HAWC2 are calculated based on the Morison equation [26] including the nonlinear hydrodynamic drag. The wave kinematics including regular and irregular airy waves are calculated through the external DLL (Dynamic Link Library) and used within the HAWC2 code. The HAWC requires hydrodynamic coefficients as input. The drag and inertia coefficients depend on the cross-sectional area of the SPAR and given in offshore standards such as DNV-OS-J101 [27]. Nonlinear restoring forces from the mooring system are calculated from a quasi-static mooring-line module that accounts for the elastic stretching of an array of homogenous slack catenary lines with seabed interaction. The natural frequencies and periods of 6DOF rigid boy motion of the selected spar platform are listed in Table 1.

Table 1. Natural frequencies and periods for rigid body motions of spar WT

	Surge	Sway	Heave	Roll	Pitch	Yaw
$\omega_n\ [rad/sec]$	0.0503	0.0503	0.2027	0.2094	0.2094	0.7854
$T_n\ [sec]$	125	125	31	30	30	8

Wind Turbine Controller

Figure 2 illustrates the controller levels for a variable-speed pitch regulated wind turbine. In practice two controller levels with different bandwidths can be considered, doubly-fed induction generator (DFIG) controller with fast dynamic response, and wind turbine controller with slow dynamic response. The wind turbine controller provides the reference pitch set-point β_{ref} to the pitch system and power set-point P_{set} to the DFIG control. The DFIG controller provides the electrical torque τ_{ref} on the generator according to the reference power.

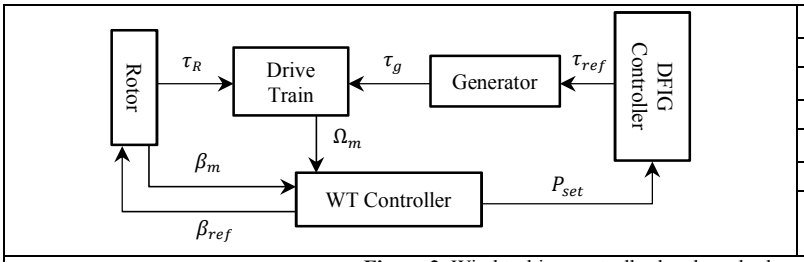

τ_g	Generator Torque
τ_R	Rotor aerodynamic torque
τ_{ref}	Torque reference
P_{set}	Power set-point
β_{ref}	Pitch angle reference
β_m	Pitch angle measurement
Ω_m	Rotor speed measurement

Figure 2. Wind turbine controller levels and relevant signals

The very fast dynamics of the DFIG control loop can be ignored and is modeled as a generator torque controlled directly by the wind turbine controller. The operational region from cut-in wind speed to cut-out wind speed is divided into below-rated and above-rated wind speed regions. In the below rated wind speed region the controller strategy is to capture the maximum power by keeping the tip speed ratio λ_{opt}=0.36 and pitch angle $\beta_{opt} = 0\ deg$. In this region, the blade pitch controller is not working and the maximum power is achieved by adjusting the generator torque as a tabulated function of filtered shaft speed. The filter is of first order with time constant 4 sec to remove the free-free drive train vibration signal. In above-rated wind speed, the generator torque is constant and the controller tries to maintain constant shaft speed. The error between the filtered measured generator speed Ω_f and the rated generator speed Ω_{rat} is sent to the PI speed controller. The output of this PI-controller is used as a reference pitch signal β_{ref} to the pitch system. A gain scheduling control of the pitch angle is implemented to compensate for the existing non-linear aerodynamic characteristics. The proportional (KP) and integral (KI) gains are defined as below,

$$KP(\beta) = KP_0.KG(\beta)\ , \qquad KI(\beta) = KI_0.KG(\beta), \qquad KG(\beta) = \frac{1}{1+\beta/KK} \tag{2}$$

where $KK = 0.11$ is the pitch angle where the gain function is equal to 0.5 for the NREL 5MW wind turbine. The pitch servo is modeled as a second order system with the natural frequency of 3 rad/sec and damping ratio of 0.9. To get the realistic response in the pitch angle control system, the servo mechanism model accounts for the pitch angle limit of [0,90] *deg* and pitch rate limit of $\pm 8\ deg/sec$. The same controller as FWT is used for LWT, with the following modifications. In the above-rated wind speed the constant power strategy is used for LWT instead of constant torque for FWT. In addition the constant proportional and integral (KP_0 , KI_0) gains of the FWT controller are increased to (0.019 , 0.008) as compared to (0.006 , 0.001) [15].

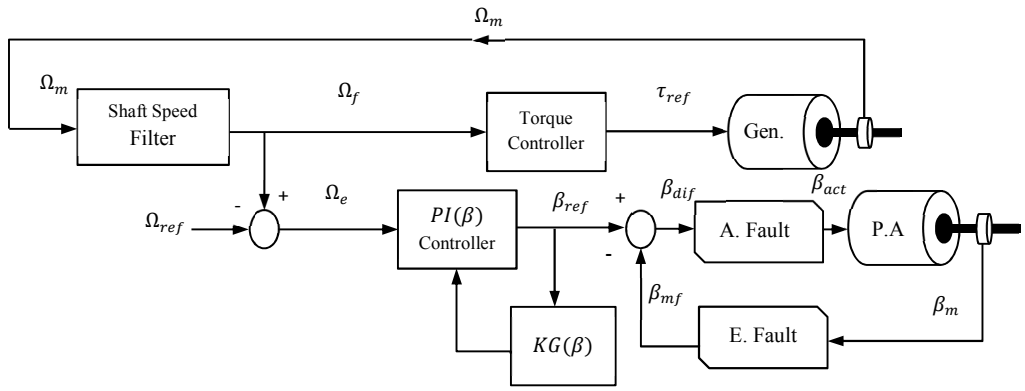

E : Encoder, **P.A**: Pitch Actuator, **A**: Actuator, **Gen.**: Generator

Figure 3. Fault Implementation in HAWC2

A block diagram of the controller is illustrated in Figure 3. This Figure shows how the faults were implemented in the controller loop. To simulate encoder faults, the fault model was placed on the path of the pitch sensor measurements. Pitch actuator faults are simulated by injecting a fault before the pitch actuator block. The mathematical models of the faults are shown in Table 2. To include the fault development time T_t, linear transition functions were defined from fault-free $(t < TTF)$ to fault-condition, as listed in Table 2. The value of T_t was selected such that the pitch rate after TTF remains below the maximum pitch rate ($\pm 8\ deg/s$). Under PAST, before the TTF the pitch actuator command is $\beta_{act} = \beta_{dif}$. After the TTF, β_{act} is shifted to the fault amplitude β_{F0} with a linear slope $(\beta_{F0} - \beta_{dif}(TTF))/(T_t)$. The slopes for PSBF and PSFV are shown in Table 2.

Table 2. Mathematical Model of Faults

Fault Type	$t \leq TTF$	$TTF < t \leq TTF + T_t$	$t > TTF + T_t$
PAST	$\beta_{act} = \beta_{dif}$	$\beta_{act} = (t - TTF)/T_t \cdot (\beta_{F0} - \beta_{dif}(TTF)) + \beta_{dif}(TTF)$	$\beta_{act} = \beta_{F0}$
PSBF	$\beta_{mf} = \beta_m$	$\beta_{mf} = \beta_m(t) + (t - TTF)/T_t \cdot \beta_{F0}$	$\beta_{mf} = \beta_m + \beta_{F0}$
PSFV	$\beta_{mf} = \beta_m$	$\beta_{mf} = (t - TTF)/T_t \cdot (\beta_{F0} - \beta_m(TTF)) + \beta_m(TTF)$	$\beta_{mf} = \beta_{F0}$

(β_{F0}: $fault\ amplitude$, β_m: $pitch\ sensor\ measurement$, β_{mf}: $sensor\ output$)

Simulation and Results

Load case setup and sensitivity analysis

The IEC 61400-3 design code [28] is used to define the required load cases in this study for FWT. In particular, the "power production plus occurrence of controller system fault" is one of the design load cases in the IEC-61400-3 for offshore wind turbines. A range of wind speeds from 5 m/s to 25 m/s (cut-out) is divided to 11 equal bins with the bin size of 2 m/s. A wind turbine class CI with the reference turbulence intensity of $I_{ref} = 12\%$ and the reference wind speed of $V_{ref} = 50\ m/s$ is selected for this analysis. The turbulence intensity is calculated as a function of U_m and the expected value of H_s and T_p are calculated for a given U_m based on the joint distribution, mentioned earlier. The reference wind speed for the sea state distribution is the wind speed at 10 m above the still water level, while the wind speed used for wind turbine simulation is defined at the hub height. Therefore the

exponential shear profile with exponent 0.14 is used to estimate the wind speed at 10 m above the still water level given the wind speed at the hub-height. For each fault case 5 different fault amplitudes (β_{F0}), including zero fault amplitude for fault-free (Reference) load case, are defined which are β_{F0} =(0, 2, 5, 7, 11) deg. The total time length of each load case is 4300 sec. Data recording starts at $t = 400\ sec$ to get rid of the initial transient effect. Thus the 3900 sec of simulation time are used for the analysis. The fault is initiated at $TFF = 200\ sec$. Investigation of the response under fault condition with steady wind shows that the transient effect of faults is always limited to the first 100 *sec* after fault occurrence. Therefore, to neglect the transient part of the simulation after fault initiation, 100 sec of the time series after TFF is neglected and the remaining 1 hr of the time series is considered to be steady state under fault conditions and is used for statistical analysis. The combination of 11 mean wind speeds and 5 fault amplitudes for each fault case results in 44 fault load cases and 11 fault-free load cases. To reduce the statistical uncertainties in the calculations, six realizations of each load case with six different seed numbers are simulated. The defined set of load cases and their wind speeds and fault amplitudes are listed in Table 3. These load cases are analyzed for each of the three fault cases (PAST, PSBF, PSFV) considered in this paper. The turbulence intensity, H_s and T_p for each U_m are listed in Table 4.

Table 3. Set of load cases and relevant mean wind speeds and fault amplitudes for (Time length=1hr X 6 seeds)

$\beta_{F0}\ [deg] \setminus U_m$[m/s]	5	7	9	11	13	15	17	19	21	23	25
0	RC1	RC2	RC3	RC4	RC5	RC6	RC7	RC8	RC9	RC10	RC11
F1=2	LC1	LC2	LC3	LC4	LC5	LC6	LC7	LC8	LC9	LC10	LC11
F2= 5	LC12	LC13	LC14	LC15	LC16	LC17	LC18	LC19	LC20	LC21	LC22
F3=7	LC23	LC24	LC25	LC26	LC27	LC28	LC29	LC30	LC31	LC32	LC33
F4=11	LC34	LC35	LC36	LC37	LC38	LC39	LC40	LC41	LC42	LC43	LC44

Table 4. Sea state and turbulent intensity for each mean wind speed

U_m[m/s]	5	7	9	11	13	15	17	19	21	23	25
I [%]	22	19	16	15	14	13	13	13	12	12	12
$H_s\ [m]$	2.10	2.39	2.71	3.06	3.43	3.82	4.23	4.65	5.09	5.55	6.02
$T_p\ [sec]$	9.55	9.62	9.74	9.89	10.05	10.24	10.43	10.63	10.85	11.06	11.24
$\omega_p\ [rad/sec]$	0.658	0.653	0.645	0.635	0.625	0.614	0.602	0.591	0.579	0.568	0.559

In the entire fault load cases only blade (2) is subjected to a fault. To show the effect of each fault on the pitch sensor measurement of blade (2), 400 *sec* of pitch sensor time series from LC17 are compared with the fault-free response in Figure 4. The black dash-line shows the fault-free response and colorful lines show the response under different fault conditions. Red line shows the effect of PAST on the pitch sensor measurement. The blade pitch angle jumped to 5 *deg* at TTF=200 sec. Green line shows the effect of PSBF and blue line shows the effect of PSFV. Effect of PAST and PSFV on the pitch angle sensor output was identical.

The pitch system controller is ideal in the below-rated wind speed; therefore pitch sensor faults cannot affect the response in the below-rated wind speeds. In the case of pitch actuator fault, fault can occur in the above-rated wind speed. When the rotor slows down to the below-rated wind speeds, fault can affect the response in this region. Therefore, in the below-rated wind speeds only the effect of PAST is studied. The results for two other faults (PSBF and PSFV) in the below rated wind speeds are also presented in the figures for consistency.

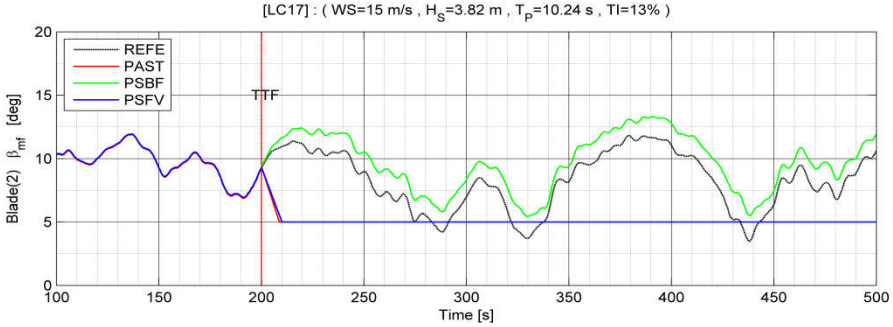

Figure 4. Pitch sensor time series of blade (2) under different fault cases (LC17) compared with fault-free response (RC6) (**FWT**)

To investigate the effects of faults on the performance of the wind turbine, effects of each fault on the rotor speed, mechanical power, aerodynamic torque and thrust are studied through the change in the mean value and standard deviation (SD) of each quantity. Shaft speed is one of the primary measurements for both wind turbine controller and safety system, therefore any change in the rotor shaft speed due to fault can affect the response of the wind turbine. Figures 5 and 6 show the effect of PAST and PSFV on the mean and SD of shaft speed for all wind speeds and fault amplitudes. Due to limited effects from PSBF on the shaft speed, results are not shown here. The reasons for the changes under fault conditions are explained when discussing the results of mechanical power.

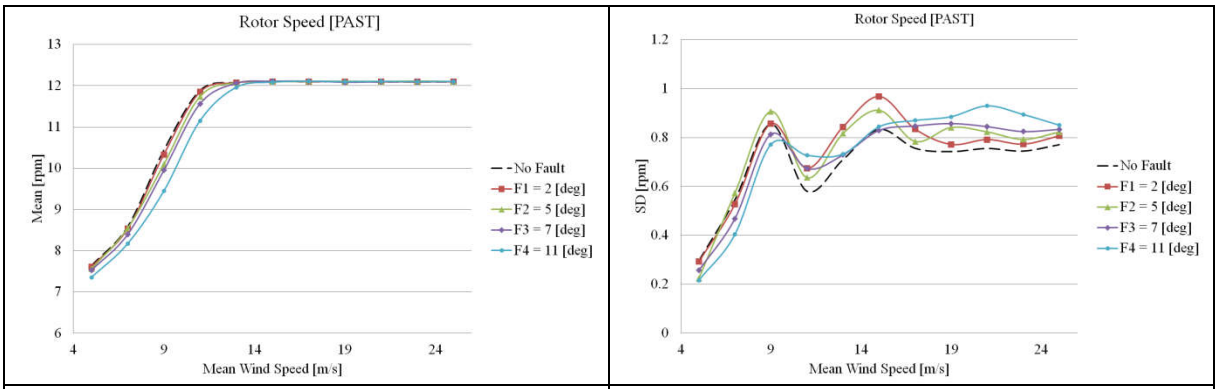

a) Mean value of rotor speed | b) Standard deviation of rotor speed

Figure 5. Effect of pitch actuator stuck (PAST) on the rotor speed (F1-F4 : Fault amplitudes) (**FWT**)

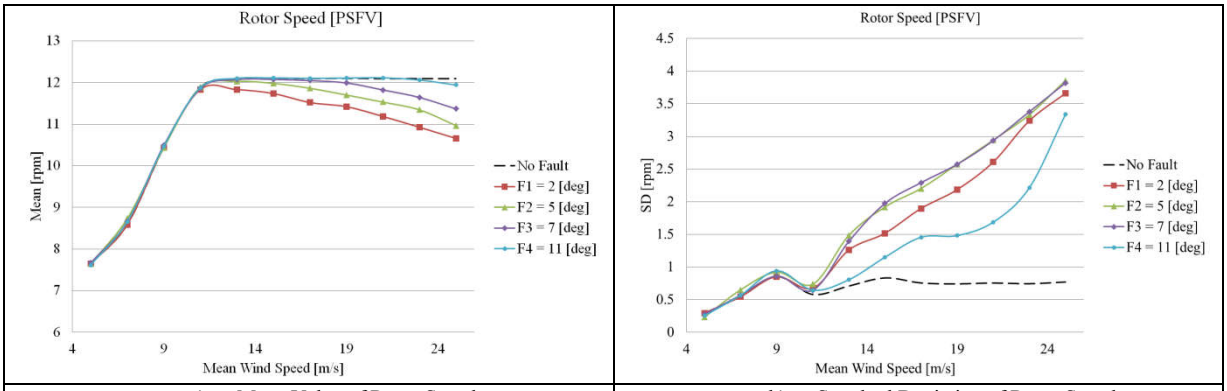

a) Mean Value of Rotor Speed | b) Standard Deviation of Rotor Speed

Figure 6. Effect of pitch sensor fixed value (PSFV) on the rotor speed (F1-F4 : Fault amplitudes) (**FWT**)

In the below-rated wind speeds, both the mean value and SD of the shaft speed were reduced due to PAST. Under PAST, the mean shaft speed was unchanged for high wind speeds. Near the rated wind speed, the rated shaft speed (12.1 rpm) was shifted to the higher wind speeds compared to the normal operation condition where the rated shaft speed was achieved at the wind speed of 11.4 m/s. The SD was increased for all wind speeds in the above rated wind speed. PSFV and PSBF had different effects on the shaft speed. Mean value of shaft speed was unchanged under PSBF in the above-rated wind speeds while it was reduced under PSFV. The SD was increased under both PSBF and PSFV while PSFV had much severe effect. Figures 7 and 8 show the effects of faults on the mean value and SD of rotor mechanical power.

The effects of faults on the mean rotor power were almost the same as the effects of faults on the rotor speed mean values. Mean value of rotor mechanical power was reduced under PAST in the below rated wind speeds and the rated power was shifted to the higher wind speeds. Until the rated power is reached, the pitch controller is not activated even though the wind speed is higher than the original rated wind speed. The SD of the power was only reduced in the below-rated wind speeds and peak of the power SD was shifted to the higher wind speeds under PAST. Comparison of Figure 7 (a) and Figure 7 (b) shows that this peak point in the power SD is correlated with the start point of the rated shaft speed. PSBF had very limited effects on the mean value and SD of the power. According to Figure 8, PSFV had much bigger effect on the power SD than on mean value. The mean value of the

power was reduced and this effect was increased at higher wind speeds. The main reason is that with increase in wind speed, the blade pitch angle is increased and the difference between the fault amplitude and actual blade pitch angle was increased. The power is a product of rotor speed and rotor torque, therefore based on the effects of the faults on the shaft speed and power, the effect of faults on the aerodynamic torque can be predicted.

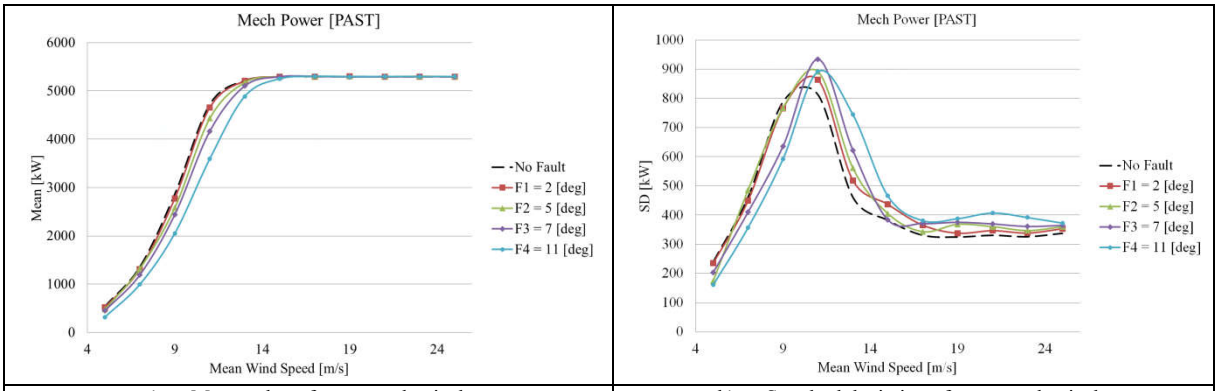

a) Mean value of rotor mechanical power b) Standard deviation of rotor mechanical power

Figure 7. Effect of pitch actuator stuck (PAST) on the rotor mechanical power (F1-F4 : Fault amplitudes) (**FWT**)

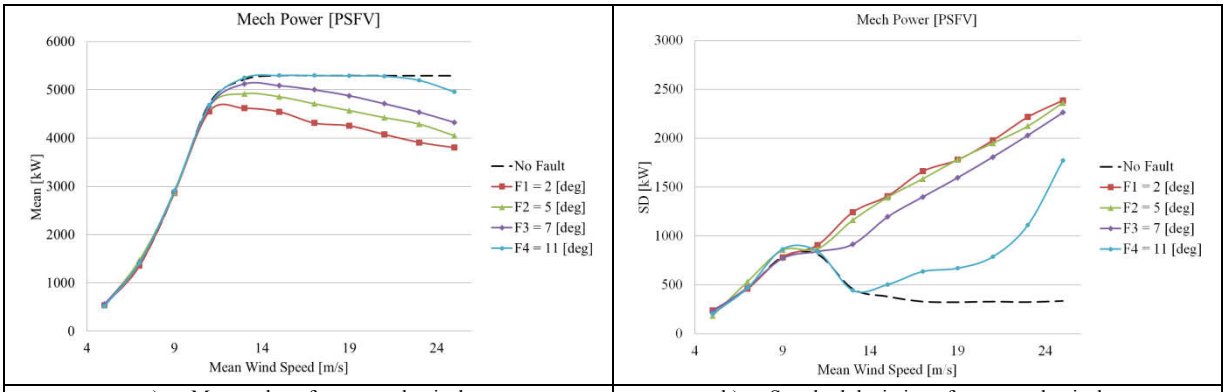

a) Mean value of rotor mechanical power b) Standard deviation of rotor mechanical power

Figure 8. Effect of pitch sensor fixed value (PSFV) on the rotor mechanical power (F1-F4 : Fault amplitudes) (**FWT**)

Figures 9 and 10 show the effect of faults on the rotor aerodynamic thrust. The rotor thrust is important for tower vibration and global motion of the platform. In the below-rated wind speeds PAST reduced the thrust and in the above rated wind speed, the peak of the thrust was shifted to the higher wind speeds and thrust was increased after the wind speeds higher than 14 m/s. According to these results, less motion and vibration is expected in the below rated wind speed under PAST, while motion and vibrations in the above rated wind speeds are expected to be increased. The PSBF had a minor effect on the thrust. The mean value and SD of the thrust were greatly increased by PSFV. This can result in very big structural responses.

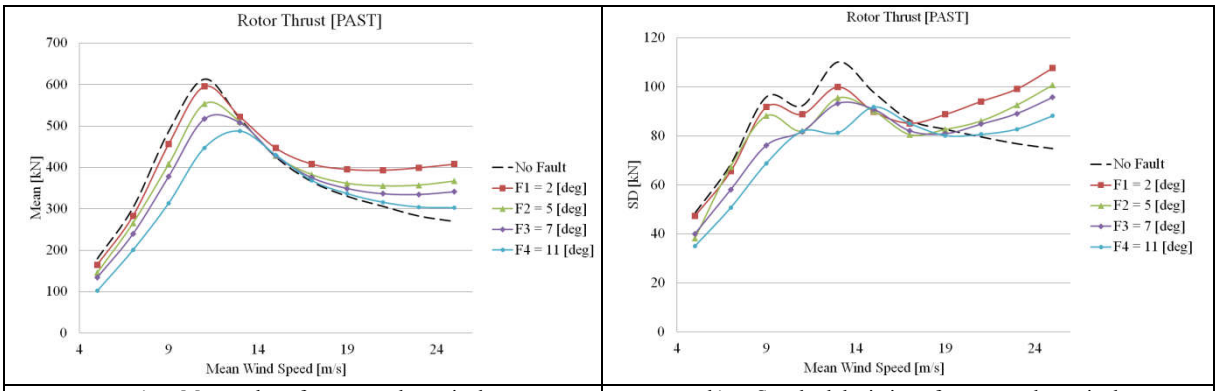

a) Mean value of rotor aerodynamic thrust b) Standard deviation of rotor aerodynamic thrust

Figure 9. Effect of pitch actuator stuck (PAST) on the rotor aerodynamic thrust (F1-F4 : Fault amplitudes) (**FWT**)

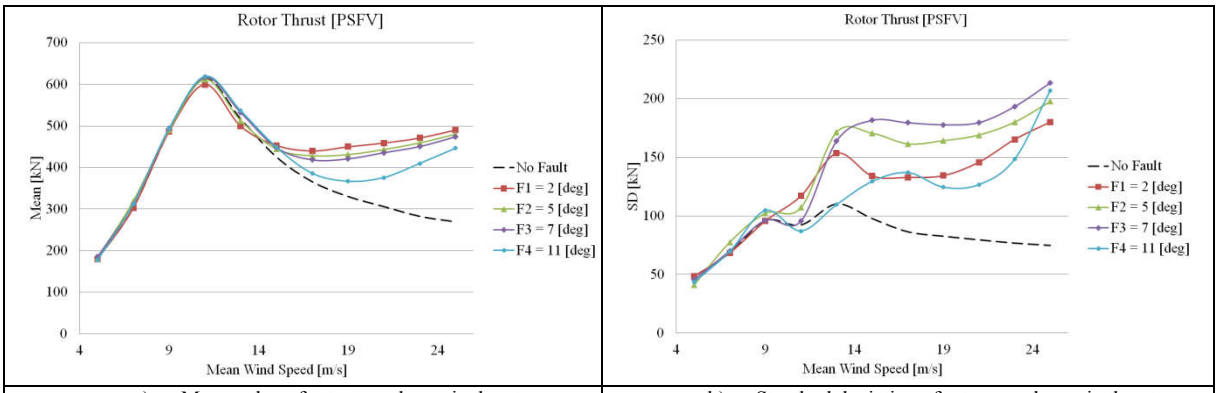

a) Mean value of rotor aerodynamic thrust

b) Standard deviation of rotor aerodynamic thrust

Figure 10. Effect of pitch sensor fixed value (PSFV) on the rotor aerodynamic thrust (F1-F4 : Fault amplitudes) (**FWT**)

To investigate how each fault case affects the performance parameters of the wind turbine, the effect of fault in blade (2), were evaluated on the two other blades. The collective blade pitch controller with individual pitch sensor measurement is used for this simulation. The pitch angle reference is only calculated based on the shaft speed error. This means the sensor measurements of blade (2) does not affect the two other blades directly. When fault occurs in blade (2), the aerodynamic torque is changed and consequently the shaft speed is changed, therefore the controller will change the pitch angle set point to adjust the shaft speed to the reference value (12.1 *rpm*). In Figure 11 the pitch angle time series of blades (1) and (2) are compared under all three fault cases for LC17. The mean wind speed for LC17 is 15 *m/s*. The blade pitch angle set point for this wind speed is 8 *deg*. The effects of faults on the pitch angle of blade (3) in all of these fault cases were similar to the blade (1), therefore only the results for blade (1) are illustrated.

In PAST (red line), blade (2) moved to 5 *deg* pitch angle at TTF=200 *sec*. The shaft speed was reduced and controller changed the pitch angle of two other blades to keep the shaft speed constant. The mean value of pitch angle in blade (1) was increased to 9.5 *deg* which was half of the change in blade (2). This means, the sum of the changes in blade (1) and (3) was equal to the total change in blade (2) with the opposite sign. This can make a big imbalanced load on the shaft. Green lines show the effect of PSBF. In this case blade (2) still followed the controller reference point with -5 *deg* constant bias. Comparison of blade (2) pitch angle with blade (2) pitch sensor measurements in Figure 4, shows that the pitch angle went to the opposite direction of pitch sensor measurement. The mean value of pitch angle in this case was 5 *deg*. Effect of PSBF on blade (1) is similar to the effect of PAST.

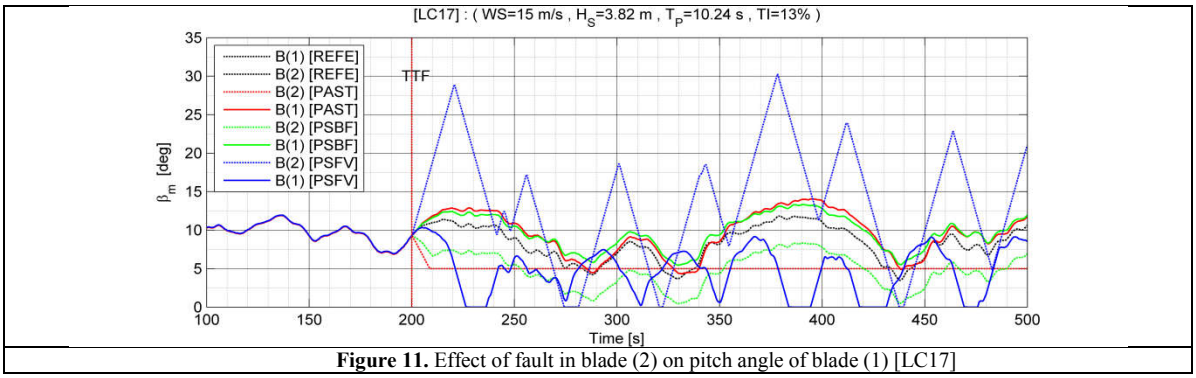

Figure 11. Effect of fault in blade (2) on pitch angle of blade (1) [LC17]

Under PSFV, the system starts to oscillate exhibiting a slow (30-50 sec) limit cycle. In the fault condition, the mean pitch angle in blade (2) was increased to 13 *deg* while the mean pitch angle of blade (1) was reduced to 4.5 *deg*. Comparing Figures 4 and 11 shows that, while there is a large oscillation in the actual pitch angle of blade (2), the pitch sensor shows a constant value. The big SD in the responses under PSFV is mainly due to this oscillation.

In fault-free operation conditions there was no difference between the pitch angles of three blades. Consequently, the bending moment on the shaft is mainly due to the tower shadow and gravitational

load on the blades. Therefore the mean values of shaft bending moments are zero. Under fault condition, there was a difference between the pitch angle of blade (2) and two other blades which makes a big change in the shaft bending moments. This difference brings a cyclic bending moment on the shaft. This bending moment on the shaft increased the torsional moment on the tower.

Floater Response

The rigid body motions of the FWT are excited by wave loads on the floater, rotor aerodynamic loads and tower drag forces. The motions in surge and sway are limited by the catenary mooring line system, while the pitch and roll motions are ballast-stabilized. As shown in the previous figures, under PAST both the mean value and SD of aerodynamic thrust in the below rated and at the rated wind speeds were reduced. As compared to the reference case, in the high wind speeds aerodynamic thrust was increased. For two other fault cases the mean value of aerodynamic thrust was almost unchanged at the rated wind speed and SD was increased specially for PSFV. At high wind speeds both the mean value and SD were increased. Change in the thrust force directly affects the surge and pitch motions of the platform. The yaw motion of the spar is mainly excited by the bending moment on the shaft which is transferred to the tower top through the shaft main bearing and gear box stands. The natural frequency and period for 6DOF rigid body motions of the SPAR platform is listed in Table 1.

In the following figures the effects of all faults on the spectra of the motion responses, for LC17, are presented. The mean wind speed for LC17 is 15 *m/s* which is in the above-rated wind speed. The wave peak spectral frequency for this wind speed is 0.61 rad/s. Figures 12 shows the spectra of surge and pitch motions for 1hr steady-state part of the time series, neglecting the transient effect of the faults. The spectra of surge motion had three peaks. The first peak was at 0.05 rad/s which belongs to the surge natural frequency. This response was mainly excited by wind loads. The second peak was at 0.2 rad/s which was pitch-induced surge motion at mean water level due to wind speed. The third peak, at 0.6 rad/s, was the wave frequency response due to wave loads. The wind-induced resonant surge response was reduced under PAST and PSFV. The pitch-resonant response was extremely increased under PSFV. The pitch spectra response had two peaks. The first peak belongs to the pitch natural frequency at 0.2 rad/s and the second peak was for the wave frequency response at 0.6 rad/s. Under fault conditions the pitch frequency response was affected. The PSFV had a big effect on the surge and pitch motions compared to the two other faults. The pitch motion was more sensitive to the faults compared to the surge motion.

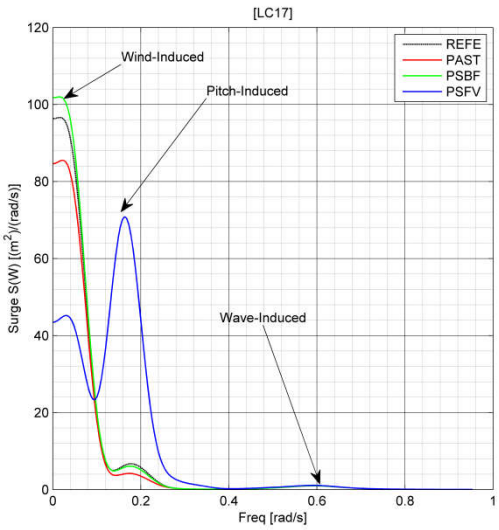

a) Surge Spectra LC17

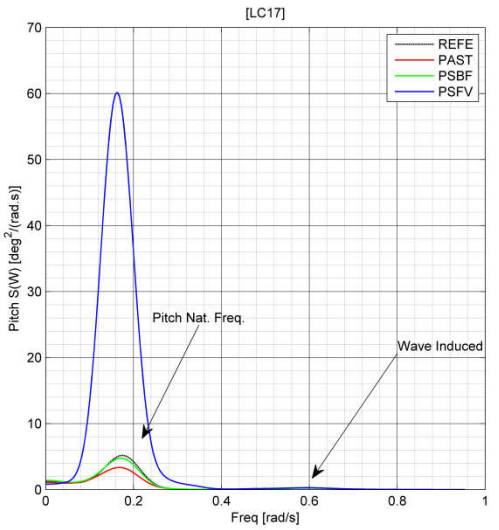

b) Pitch Spectra LC17

Figure 12. Effect of controller faults on surge and pitch motions (1hr- steady state, $U_m = 15$, $H_s = 3.82$, $T_P = 10.24$)

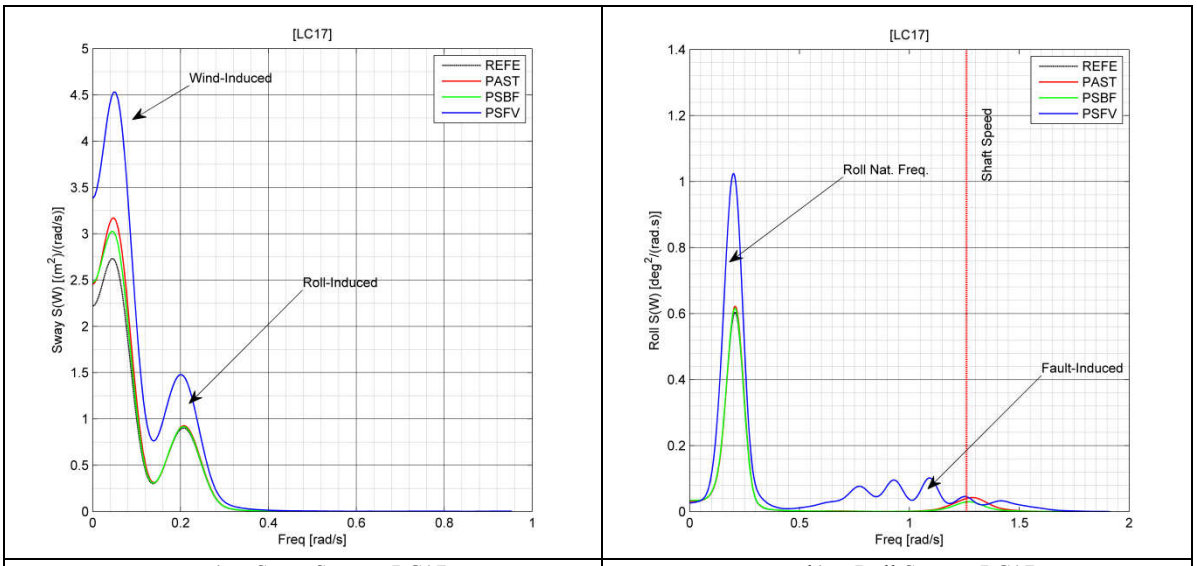

a) Sway Spectra LC17 b) Roll Spectra LC17

Figure 13. Effect of controller faults on sway and roll motions (1hr- steady state, $U_m = 15$, $H_s = 3.82$, $T_P = 10.24$)

Figure 13 shows the effect of faults on the sway and roll motion responses, which are induced by side to side forces on the tower. These forces mainly come from the forces on the main shaft and turbulent wind components in the lateral direction. The sway and roll amplitudes were much smaller than the surge and pitch motions. In the LC17 the wind and wave were coaxial and normal to the rotor plane. Therefore there was no side to side force from the wave on the substructure. As one can see from the Figure 13 both the sway and roll motions were affected by fault. The effects of faults on the roll and sway motions are negligible due to small amplitudes of these responses.

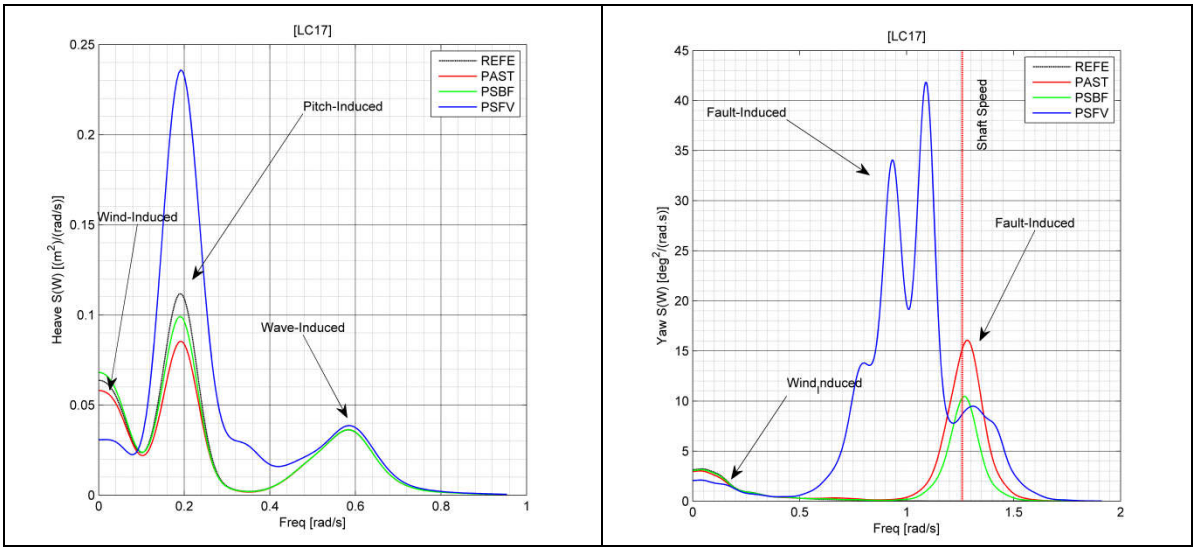

a) Heave spectra LC17 b) Yaw spectra LC17

Figure 14. Effect of controller faults on heave and yaw motions (1hr- steady state, $U_m = 15$, $H_s = 3.82$, $T_P = 10.24$)

Figure 14 shows the heave and yaw responses of the floater under three fault cases. The heave response is mainly induced by wave loads. The heave natural frequency is 0.2 *rad/s*. There were three peaks in the heave response spectra. The first peak at 0.05 was related to the wind-induced response. The second peak at 0.2 *rad/s* was the pitch natural frequency. The heave motion in this frequency is due to pitch motion. The third peak was related to the wave frequency response. In the above rated wind speeds both PAST and PSBF reduced the heave amplitude. The PSFV increased the heave response. While the maximum effect was closed to the natural frequency but the response at higher frequencies was also excited. The spar platform has low yaw mooring stiffness. In addition, the moment of inertia around the tower Z axis is small. Therefore yaw motion can be excited by a small

yaw moment. Due to the cylindrical shape of the floater, waves cannot induce platform yaw motion. The yaw moment on the platform was mainly due to the yaw misalignment and imbalance load on the rotor. Under fault conditions the bending moments on the shaft were increased which led to the bigger yaw moment. A comparison between yaw motion peak frequency and shaft speed shows that the peak of the yaw response appeared at rotor rotational speed (1P effect). For the PSBF and PAST the bandwidth of yaw response was narrower than the response under PSFV. This effect comes from the large SD of the shaft speed and blade pitch angle under PSFV.

Structural responses

In this section the effect of faults on the extreme values as well as the mean and SD for the structural response at: tower bottom (TB), shaft main bearing (SB), yaw bearing (YB) and blade root (BR) are presented. The normal stresses on the blade root, tower bottom and shaft are calculated based on the reference structural properties of the selected NREL 5 MW wind turbine [15]. In a case where the fault is not detected in the system or the fault does not exceed the safety system thresholds, it is important to know how big the fatigue damage of the structure in the presence of the fault is. Therefore the short term fatigue damage to the structural members under fault conditions was compared with the fault-free conditions.

Six 1-hr stochastic samples were simulated for each load case to reduce stochastic uncertainty in the calculations. To study the effect of faults on structural loads, some reference values were calculated in normal operational conditions. These reference loads include: short term extreme value, expected largest mean value and SD for each load component as a well as the mean wind speeds that these max values were occurred. These values are listed in Table 5, for load cases RC1 to RC11.

Table 5. Expected max loads on the selected structural members (FWT)

Load Components	Expected Max Value	U_m	Largest Mean	U_m	Largest SD	U_m
Tower Bottom Mx kNm	152532	25	74296	11	29056	25
Tower Bottom My kNm	54265	25	14766	25	10191	25
Tower Bottom Mz kNm	13132	25	1232	25	2909	25
Yaw Bearing Mx kNm	13226	25	2575	25	2654	25
Yaw Bearing My kNm	10434	25	8451	23	1109	9
Yaw Bearing Mz kNm	13101	25	1200	25	2910	25
Shaft Mx kNm	3067	25	0	25	2758	25
Shaft My kNm	2884	17	0	25	2766	25
Shaft Mz kNm	5597	25	4180	23	549	9
Blade Root Mx kNm	14861	13	8950	11	2685	25
Blade Root My kNm	5932	11	998	11	2589	11
Blade Root Mz kNm	147	13	34	25	57	17

The expected values of loads under fault conditions were calculated and normalized by the corresponding values from the normal operation. The results are presented in Figures 15 and 16 as a ratio of fault load over normal load. The largest mean value and standard deviation of the responses for each load case are shown in the figures.

The change in the largest mean and SD for all selected structural members are plotted in Figure 15. The loads were calculated based on the local coordinate system of each component (see Figure 1). It is apparent from Figure 15 (a) that, the SD of tower bending moments was not changed as much as the SD of torsional moment and that the mean of tower fore-aft bending moment under PAST was reduced. The latter is because of reduction in peak point of the mean aerodynamic thrust under PAST. The relative change in mean shaft bending moments are not shown in the Figures because the mean values were zero without faults. PSFV had much larger effect on the vibrations (SD) compared to the two other fault cases.

Figure 16 shows the change in the extreme values. The extreme values increased for all three fault cases. The major effect was on shaft bending moment loads. In general the effect of PSFV was bigger than the two other fault cases. The extreme values under fault condition were always bigger than the normal operational condition. For example the extreme value of the tower bottom bending moment M_x was increased by 14%, 18% and 100 % under PAST, PSBF and PSFV respectively.

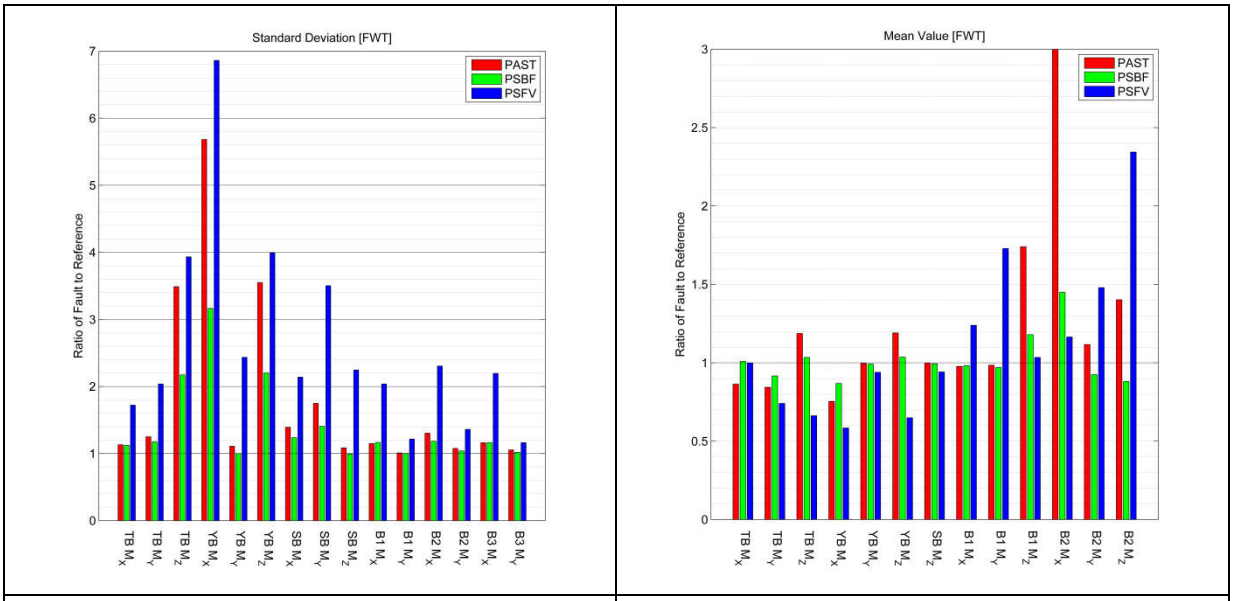

a) Standard Deviation b) Mean Value

Figure 15. Comparision of effect of faults on the Mean & SD (**FWT**)
(**TB**: Tower Bottom, **YB:** Yaw Bearing, **SB:** Shaft Bearing, **B1-B3**: Blade 1-3, **Mx:** Bending moment on X axis, **My:** Bending moment on Y axis, **Mz:** Torsional Moment on Z axis) (6 x 1hr Samples)

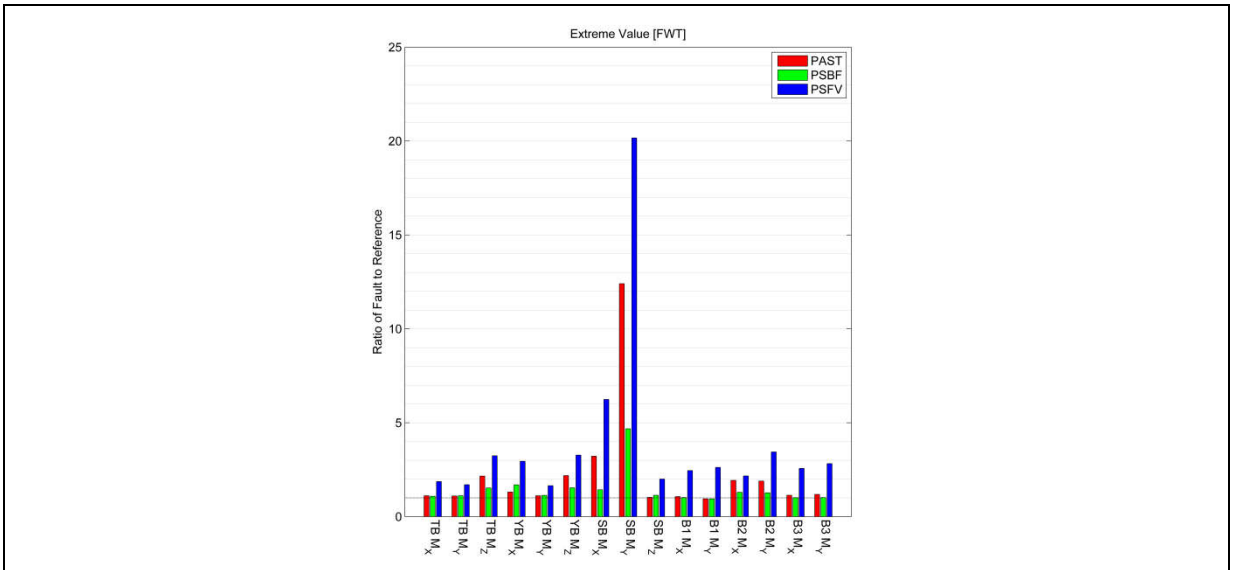

Figure 16. Comparision of effect of faults on the extreme values (**FWT**)
(**TB**: Tower Bottom, **YB:** Yaw Bearing, **SB:** Shaft Bearing, **B1-B3**: Blade 1-3, **Mx:** Bending moment on X axis, **My:** Bending moment on Y axis, **Mz:** Torsional Moment on Z axis) (6 x 1hr Samples)

The mean value of yaw bearing bending moment around Y axis was almost unchanged under fault conditions. The SD of fore-aft bending moment M_x and torsional moments M_z were increased under fault conditions. The extreme values of yaw bearing loads were all increased. Fore-aft bending moments and torsional moment were increased by more than 300% and 200% under PSFV respectively. For yaw bearing the main effect was on the SD and vibrations.

The mean values of shaft bending moments are zero under normal operational conditions. Both the mean value and SD of shaft torque M_z remained unchanged under PAST and PSBF. The mean values of shaft loads were more sensitive to the faults than SD. The extreme loads under fault conditions can be 3 to 20 times larger than normal operational conditions.

The reference load characteristics on all three blades were almost equal. Under normal operational condition, the flapwise bending moment M_x was the dominant load. The mean value of loads on the blade (2), which was subjected to fault, was increased under all fault conditions. PSBF had very small effect on the mean value and SD of two other blades. The extreme values of blade loads were more

sensitive to PSFV compare to the other fault cases. As mentioned before, only blade (2) was subjected to faults. Under PAST and PSBF, the extreme loads on the blade (2) were bigger than two other blades while under PSFV flapwise bending moment on blade (2) was smaller than two other blades.
To compare the extreme values under fault conditions with other potential extreme responses, two additional conditions from IEC were calculated. These extreme responses include the operation under extreme turbulent model (ETM) (DLC 1.3)[28] and the parked condition under extreme environmental conditions with the 50 years recurrence period. The extreme wind speed and sea state with recurrence period of 50 years was calculated with contour line method [29] for the selected offshore wind site. The extreme conditions based on maximum mean wind speed and maximum significant wave height were calculated and listed in Table 6. For parked conditions, two rotor azimuth positions were considered: Blade (1) is pointed upward and blade (1) is pointed downwards.

Table 6. Environmental conditions on the 50-years contour surface with maximum U_{10m} and maximum H_s

Conditioned on	U_{10m}	H_s
$U_{hub}\ [m/s]$	45	42.5
$H_s\ [m]$	13.5	15.3
$T_P\ [sec]$	15	15.5

Table 7 compares the short term extreme responses under fault conditions with extreme response under normal operation, ETM and parked conditions. For the tower bending moment, the parked condition was the dominant load case. For the tower torsion, PSFV was the dominant extreme load case. For shaft bending moment as well as blade bending moments, the extreme response under fault cases was bigger than other load cases. In the next section, effects of faults on the short term fatigue damage of wind turbine structure are evaluated.

Table 7. Comparison of Fault and Fault-free Extreme response (FWT) (6 x 1hr Samples)

Load Components	Normal Operation	Parked	ETM	PAST	PSBF	PSFV
Tower Bottom Mx kNm	152532	301003	174457	177602	182423	291928
Tower Bottom My kNm	54265	97714	72163	62788	65481	94136
Tower Bottom Mz kNm	13132	8371	15720	30033	26944	45490
Yaw Bearing Mx kNm	13226	8272	18048	30437	29352	69520
Yaw Bearing My kNm	10534	23039	11139	11724	13006	20454
Yaw Bearing Mz kNm	13101	2512	15703	30366	27173	45879
Shaft Mx kNm	3067	14633	15256	18002	5292	38129
Shaft My kNm	2884	6500	16297	37560	24580	53414
Shaft Mz kNm	5597	23198	6168	5685	5508	7250
Blade Root Mx kNm	14861	14177	18060	27243	16042	34157
Blade Root My kNm	5932	11210	7992	11737	8910	18989
Blade Root Mz kNm	147	449	215	226	488	1335

Effect of Faults on the Fatigue Damage
According to the IEC61400-3, if occurrence of fault does not lead to immediate shut down of the wind turbine then the resulting fatigue damage should be evaluated. The rainflow counting method [30] was used to investigate the change in the number of cycles and amplitude of loads under fault conditions. The effects of faults on the short term fatigue damage of shaft, tower and blades root were estimated through the calculation of normal stresses (S_{zz}) on each component. The normal stress S_{zz} is induced by bending moments (M_x , M_y) and axial force (F_z). The linear SN curve with fixed SN slopes of 3, 6 and 4 are used to calculate the fatigue damage of tower, blade root and shaft respectively. For each load case the short term (1 hour) fatigue damage for a given mean wind speed (i) and fault amplitude (j) was calculated which is indicated by D_{ij}. At each mean wind speed the mean value of fatigue damage D_i for all four fault amplitudes was calculated as representative of expected fatigue damage for each fault case at a given mean wind speed.

$$D_i = \frac{1}{4}\sum_{j=1}^{4} D_{ij} \quad , i : wind\ speed\ index(1-11)\ , j : fault\ amplitude\ index\ \ (1-4) \tag{3}$$

The expected fatigue damage at each wind speed was weighted by probability of mean wind speed (P_i) for the selected wind turbine site. The shape and scale parameters for wind speed Weibull distribution are 1.708 and 8.426 respectively. The accumulated fatigue damage for 1-hour working under each mean wind speed were calculated for all three fault cases and compared with the reference load cases.

$$D_T = \sum_{i=1}^{11} P_i D_i \quad , \quad i : wind\ speed\ index(1-11) \tag{4}$$

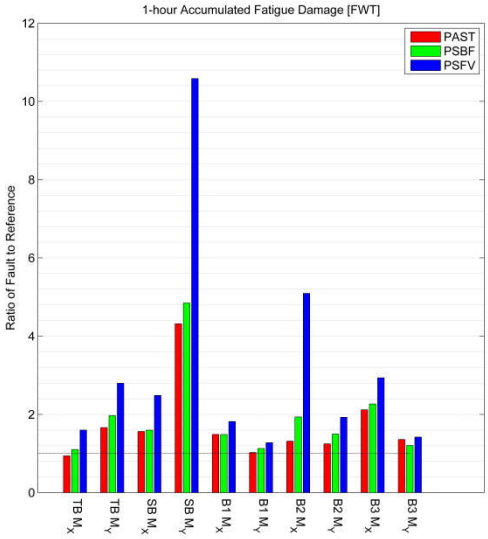

Figure 17. Comparision of accumulated fatigue damage due to faults (**FWT**)
(**TB**: Tower Bottom, **SB:** Shaft Bearing, **B1-B3**: Blade 1-3, **Mx:** Bending moment on X axis, **My:** Bending moment on Y axis

Figure 17 shows the ratio of accumulated fatigue damage under fault condition to the non-fault condition. In general the fatigue damage under sensor faults was bigger than actuator fault. This is because in the bellow rated wind speed, the loads were reduced under PAST and unchanged under two other fault cases. Therefore the fatigue damage in the bellow rated wind speed was reduced under PAST and consequently reduced the contribution of PAST in the accumulated fatigue damage compared to the PSBF and PSFV.

The shaft was the most sensitive structural member for fatigue damage. The fatigue damage under PSFV was ten times the normal operation condition. Increase in fatigue damage due to side-to-side bending moment M_y on the tower was bigger than the fore-aft bending moment M_x. This is because the M_y bending moment is induced by shaft bending moments while M_x is mainly induced by thrust force. As shown before the change in the shaft bending moments was the biggest change compared to the other load components. Increase in the fatigue damage on the blades was different from each other. Increase in the fatigue damage due to flapwise bending moment was bigger than edgewise bending moment on all three blades. Under PAST fatigue damage on blade (2) was less than blade (1) and (3). This is because, under fault condition blades (1) and (3) were pitched in the opposite direction of blade (2) and loads were increased on two other blades compared to the blade (2). Under PSBF fatigue damage of blade (3) due to flapwise bending moment was bigger than blade (1) and (2).

Table 8. The relative change in the accumulated fatigue damage of substructures due to 1-hr working under fault

	PAST		PSBF		PSFV	
Order	Component	FDRD	Component	FDRD	Component	FDRD
5	Shaft	251 %	Shaft	391 %	Shaft	972 %
4	Tower	83 %	Blade 3	127 %	Blade 2	415 %
3	Blade 3	68 %	Tower	101 %	Blade 3	194 %
2	Blade 1	34 %	Blade 2	96 %	Tower	185 %
1	Blade 2	12 %	Blade 1	46 %	Blade 1	79 %

FDRD : fatigue damage relative difference in percent

Based on the previous results the components are sorted according to the change in the magnitude of fatigue damage to the structure for each fault case. In this regards the average relative difference of fatigue damage in the above rated wind speeds for each structural member is calculated and components are sorted in the descending order in Table 8.

Comparison of Transient and Steady State Effect of Faults on the Extreme Response

In this section, effects of two time characteristics of fault on the results are studied. The first one is the transient effect of fault compared to the steady state effect of fault. As mentioned earlier, transient effect of fault was damped out in the first 100 sec after TTF. Therefore, the maximum response in the first 100 seconds of the responses after TTF is compared with the maximum response for the rest of 1 hour time series. Afterwards, the effect of TTF or azimuth position of the rotor on the steady state response is studied and some selected results are presented. In Figure 18 the steady-state extreme response (solid-line) are compared with transient extreme response (dashed-line) for PAST. This figure shows the results for flapwise bending moment on blade (2) and shaft bending moment M_x under PAST. In the below rated wind speed the transient response for blade flapwise bending moment was slightly bigger than the steady state response because after fault the thrust load on the blade was reduced. In the above rated wind speed the transient effect was much smaller than the steady state effect due to increase in the thrust force after fault. For shaft bending moment M_x, the transient response was always smaller than the steady state response. Comparison for the other fault cases shows that, the maximum response in the first 100 second after TTF is always smaller than steady state response. A comparison between the transient and steady-state response with mean wind speed without turbulent, shows that the maximum response in the transient part is always 5 to 10 percent bigger than steady-state response but under combined mean and turbulent wind speeds the transient response is smaller. The reason is that, the wind turbine is a hybrid system [31] and the responses depend on both deterministic and stochastic parts of wind speed.

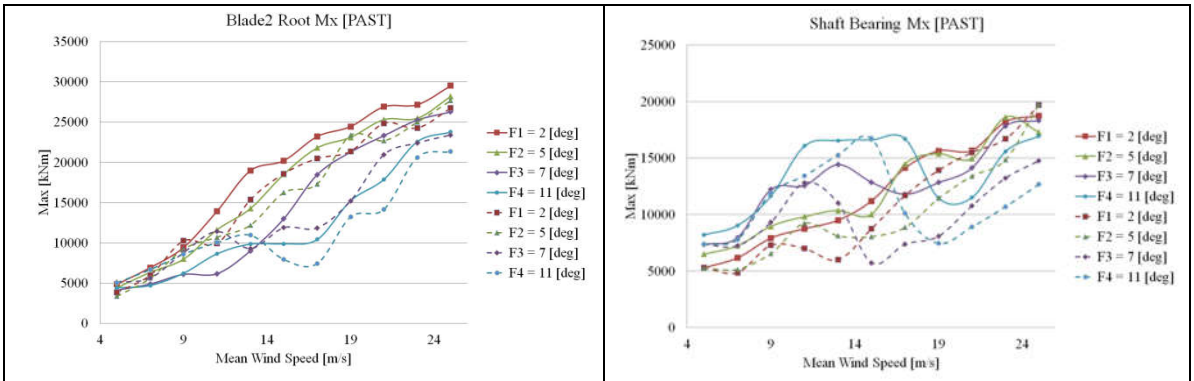

a) Blade 2 flapwise bending moment

b) Shaft bending moment Mx

Figure 18. Comparision of transient (during 100 s after TTF) and steady state (during 1-hr after TTF+100s) effects of PAST

To study the effect of TTF or azimuth position of the rotor on the results, a set of load cases including 5 mean wind speeds of (7, 11, 13, 17, 23) *m/s* with fault amplitude of 11 *deg* was considered. For each mean wind speed, faults were initiated at 11 different time instances from 600 to 610 *sec* with the time step of 1 *sec*. The max, mean value and SD of 600 *sec* of the responses after TTF were calculated and compared with each other. In Figure 19, the extreme response for shaft bending moment and blade (2) root bending moment under PAST and PSBF are illustrated respectively. Clearly these figures show that the azimuth position of the rotor had no effect on the first 600 of the response after the fault.

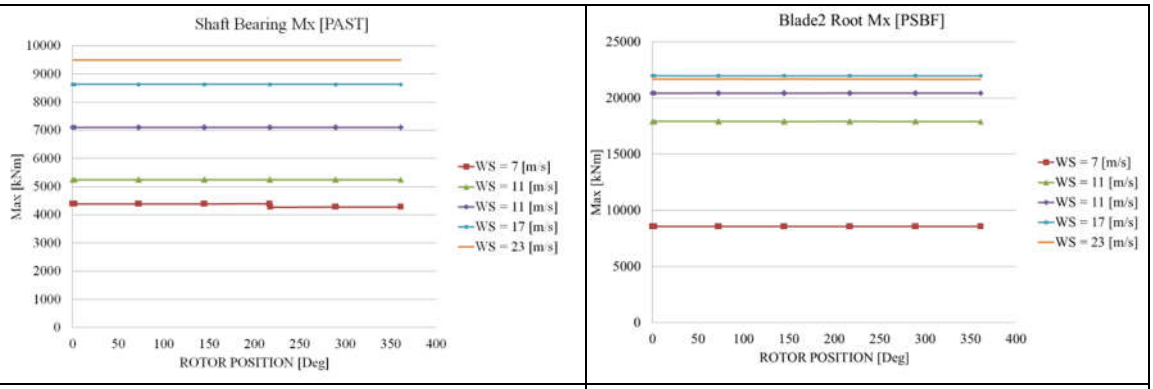

a) Shaft bending moment Mx under [PAST] | b) Blade 2 flapwise bending moment under [PSBF]

Figure 19. Effect of TTF on the max responses (during 600s after TTF) at different mean wind speed for [PAST] and [PSBF]

Comparison of Land Based and Floating Wind Turbine under Fault Conditions

In this section, the responses of a land-based wind turbine are compared with the offshore wind turbine under same fault cases. The aim is to compare the effects of faults on these two concepts. Table 9 shows the reference extreme loads for a LWT similar to the Table 5 for FWT. To generate these results, a set of load cases similar to the FWT is used with some modifications on environmental conditions. The shear profile exponent and reference turbulence intensity are increased from 0.14 to 0.2 and 0.12 to 0.14, respectively, according to the IEC 61400-1 [32].

Table 9. Expected max loads on the selected structural members (LWT) (Time length=1hr X 6 seeds)

Load Components	Expected Max Value	U_m	Largest Mean	U_m	Largest SD	U_m
Tower Bottom Mx kNm	76511	13	50065	11	10289	9
Tower Bottom My kNm	39427	25	8169	25	8216	25
Tower Bottom Mz kNm	7518	25	435	19	3165	25
Yaw Bearing Mx kNm	13967	25	5247	5	2872	25
Yaw Bearing My kNm	5664	25	4319	25	654	9
Yaw Bearing Mz kNm	5388	15	435	19	3154	25
Shaft Mx kNm	7255	19	6	19	3095	25
Shaft My kNm	5344	25	6	25	3066	25
Shaft Mz kNm	5735	25	4184	25	642	9
Blade Root Mx kNm	14776	15	8586	11	3119	25
Blade Root My kNm	7123	25	995	11	2684	13
Blade Root Mz kNm	142	11	31	11	40	13

Table 10. Comparison of Fault and Fault-free Extreme response (LWT)

(Time length=1hr X 6 seeds)

Load Components	Normal Operation	PAST	PSBF	PSFV
Tower Bottom Mx kNm	76511	157456	115970	561555
Tower Bottom My kNm	39421	101382	85895	825614
Tower Bottom Mz kNm	7518	30196	24946	80953
Yaw Bearing Mx kNm	13967	30131	15937	70680
Yaw Bearing My kNm	5664	7618	7272	24585
Yaw Bearing Mz kNm	5388	30139	24878	80142
Shaft Mx kNm	7255	21252	19144	14210
Shaft My kNm	5344	27551	14675	67374
Shaft Mz kNm	5735	5759.	5843	7889
Blade Root Mx kNm	14776	23492	15666	41752
Blade Root My kNm	7123	10838	8791	51260
Blade Root Mz kNm	103	281	216	9483

The response characteristics including extreme values, largest mean value and SD of FWT are divided by corresponding responses from LWT and presented in Figure 20(a). Based on this figure, blade loads were almost the same on both concepts. For tower bottom and yaw bearing loads, except the yaw bearing fore-aft bending moments, the loads in FWT were bigger than LWT, the reason is more dynamic loads on the tower due to the motions of the floater in FWT. The shaft loads in FWT were

smaller than LWT. This is mainly because of constant torque strategy in FWT. Figures 20(b)-21 show the change in the response characteristics of the LWT due to faults. The tower fore-aft bending moment and torsion in FWT under PAST and PSBF were bigger than LBWT. But the effect of PSFV on the tower loads in LBWT was much bigger than FWT. The effect of faults on the Yaw torsion of the LWT was bigger than FWT. This is because the yaw stiffness of LWT is larger than FWT. Faults are more severe for shaft loads in FWT compared to the LWT. However the shaft extreme loads under normal operation condition in LWT was bigger than FWT but under fault condition increase in shaft loads of FWT was bigger than LWT. PSBF and PAST almost had the same effects on the blade loads but PSFV had bigger effect on the flapwise bending moments of all three blades in LWT.

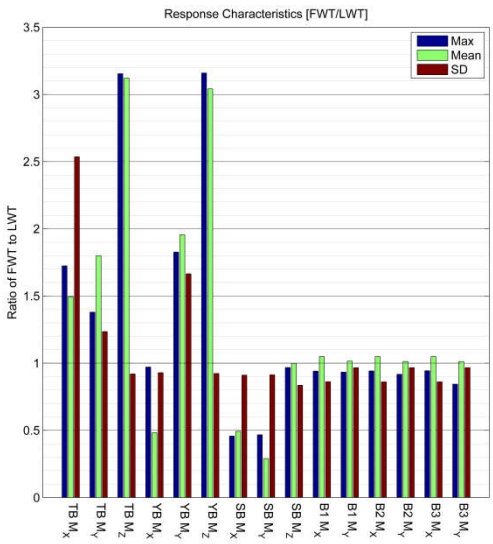

a) Comparision of responses characteristics (**LBW** and **FWT)**

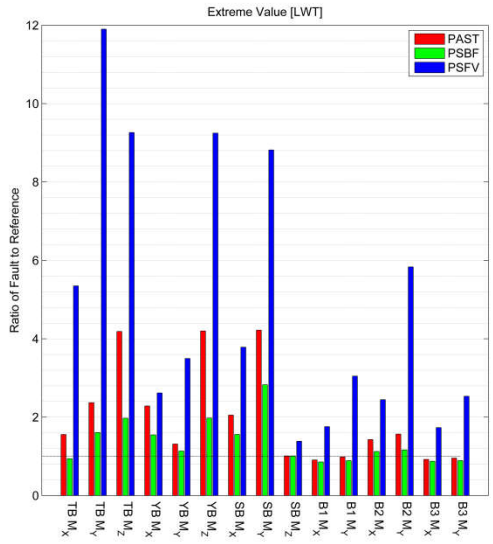

b) Comparision of effect of faults on the Extreme (**LWT**)

Figure 20. (**TB**: Tower Bottom, **YB:** Yaw Bearing, **SB:** Shaft Bearing, **B1-B3**: Blade 1-3, **Mx:** Bending moment on X axis, **My:** Bending moment on Y axis, **Mz** Torsional Moment on Z axis) (6 x 1hr Samples)

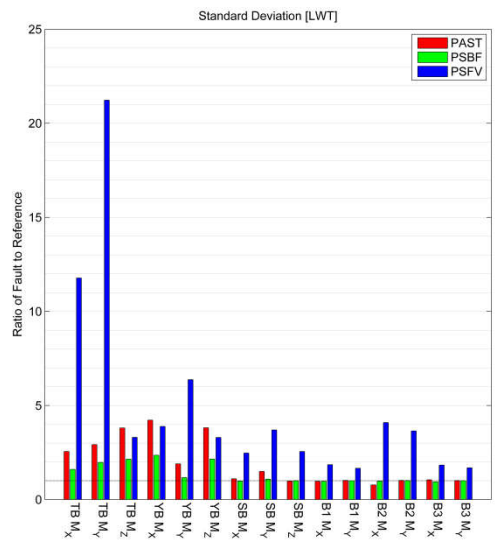

a) Standard Deviation

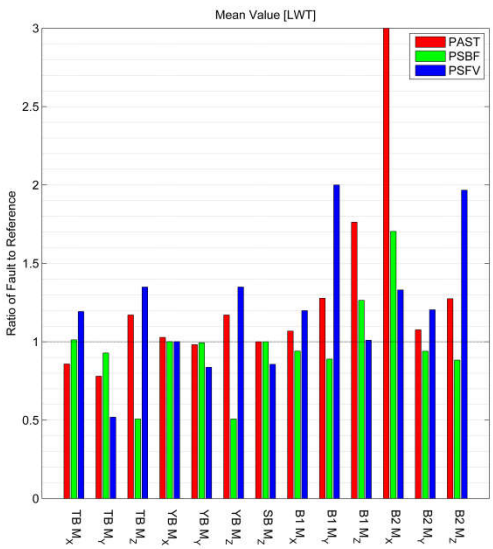

b) Mean Value

Figure 21. Comparision of effect of faults on the Mean & SD (**LWT**)

(**TB**: Tower Bottom, **YB:** Yaw Bearing, **SB:** Shaft Bearing, **B1-B3**: Blade 1-3, **Mx:** Bending moment on X axis, **My:** Bending moment on Y axis, **Mz:** Torsional Moment on Z axis) (6 x 1hr Samples)

In the following table the extreme response of the LWT and FWT under fault conditions are compared.

Table 11. Comparison of Extreme Response (LWT and FWT) (6 x 1hr Samples)

Load Components	Offshore Wind Turbine			Land Base Wind Turbine			RD [%]
	Fault Case	Magnitude	U_m	Fault Case	Magnitude	U_m	
Tower Bottom Mx kNm	PSFV	291928	25	PSFV	561555	25	80 %
Tower Bottom My kNm	PSFV	94136	23	PSFV	825614	23	692 %
Tower Bottom Mz kNm	PSFV	45490	23	PSFV	80953	25	77 %
Yaw Bearing Mx kNm	PSFV	69520	23	PSFV	70680	23	1 %
Yaw Bearing My kNm	PSFV	20454	25	PSFV	24585	23	20 %
Yaw Bearing Mz kNm	PSFV	45879	23	PSFV	80142	25	74 %
Shaft Mx kNm	PSFV	38129	25	PAST	19144	25	-49 %
Shaft My kNm	PSFV	53414	25	PSFV	67374	25	26 %
Shaft Mz kNm	PSFV	7250	25	PSFV	7889	25	8 %
Blade Root Mx kNm	PSFV	34157	25	PSFV	41752	25	22 %
Blade Root My kNm	PSFV	18989	25	PSFV	51260	21	169 %
Blade Root Mz kNm	PSFV	1335	25	PSFV	9483	23	610 %

Conclusions

The results presented in this work characterized the dynamic responses of the OC3-Hywind spar wind turbine under blade pitch controller faults. Three fault cases together in the blade pitch actuator and sensor were simulated and the effects of faults were shown on the short term extreme values and fatigue damage in different structural members. Floater responses were also investigated. Steady-state and transient effects of faults were studied. Finally a comparison was made between the floating and a land-based wind turbine under fault conditions.

Results showed that, different faults have fairly similar signature. Sensitivity analysis showed that, in below rated wind speeds, PAST reduced the responses. In the above rated wind speeds, the mean values were almost unchanged while extreme and SD were increased. Under PSFV, the responses were extremely excited due to the slow limit cycle in the controller. PSBF had the minor effect on the response compare to the other fault cases. Comparison of the transient and steady-state effects of faults showed that, the steady state extreme responses were always bigger than transient response. The extreme responses were insensitive to the azimuth position of the rotor.

Effect of faults on the responses of the floater was studied. PSFV found to be the most severe fault case for the floater response. The yaw motion was highly sensitive to all three fault cases. PAST and PSFV had limited effects on the 5 other DOF. Pitch and heave motions were also affected by PSFV.

Effect of faults on the structural responses indicated that, the shaft was the most risky component under fault condition and the extreme loads under fault conditions might be 20 times bigger than normal operational conditions. PSFV had the largest effect on all of the structural responses. Under PAST and PSBF extreme loads on the faulty-blade were bigger than two other blades while under PSFV extreme loads on the faulty-blade were smaller than the others.

Comparison of the extreme responses under fault condition with other extreme responses showed that, for blade, shaft and yaw bearing, the extreme responses under fault condition were dominate while for tower, the parked condition was the dominant load case.

Effect of faults on the short term fatigue damage of shaft was bigger than other structural members. The increased in the side-to-side fatigue damage in tower was bigger than fore-aft fatigue damage. Fatigue damage on blades was different from each-other under fault conditions and the effect was mainly on the flapwise direction fatigue damage.

The comparison between the LWT and FWT under normal operation and fault conditions showed that, in general faults caused bigger damage to the tower and yaw bearing in land based wind turbine compare to FWT and bigger damage to the shaft and blades of FWT compare to the LWT.

Acknowledgement

The authors gratefully acknowledge the financial support from the Research Council of Norway granted through the Centre for Ships and Ocean Structures, NTNU. Thanks are extended to Erin E. Bachynski and Zhiyu Jiang for their useful discussions and comments.

References

1. Wiggelinkhuizen E. J.; Braam H.; Rademakers L., V.T.W., *CONMOW: condition monitoring for offshore wind farms*, in *Wind Energy Report ECN-RX-03-036* (2003), Energy Research Centre, Netherlands.
2. Yang W.; Tavner P. J.; Crabtree C. J.; Feng Y., Q.Y., *Wind turbine condition monitoring: technical and commercial challenges.* Journal of Wind Energy, (2012), DOI 10.1002/we.1508.
3. Tavner P. J., Xiang J. and S. F., *Reliability analysis for wind turbines.* Journal of Wind Energy, (2007). **10**(1): p. 1-18.
4. Jiang Z., Karimirad M. and Moan T., *Steady State Response of a Parked Spar-type Wind Turbine Considering Blade Pitch Mechanism Fault*, in *International Offshore Polar Engineering Conference (ISOPE)*2012: Rhodes, Greece, June 17-22.
5. Cutululis N. A.; Hansen A. D., I.F., Sørensen P.,. *Grid Faults Impact on the Mechanical Loads of Active Stall Wind Turbine*. in *The Second International Symposium on Electrical and Electronics Engineering, ISEEE*. 2008. Galati, Romania, Aug 08-13.
6. Odgaard P. F.; Stoustrup J. and Kinnaert M., *Fault tolerant control of wind turbines: a benchmark model*, in *7th IFAC Symposium on Fault Detection, Supervision and Safety of Technical Processes* 2009: Barcelona, Spain, June 30 - July 3.
7. Odgaard P. F.; Stoustrup J.; Nielsen R. and Damgaard C., *Observer based detection of sensor faults in wind turbines*, in *European Wind Energy Conference* 2009: Marseille France, March 16-19.
8. Fang S., Leira B. J. and Blanke M., *Position mooring control based on a structural reliability criterion.* Structural Safety, 2013. **41**: p. 97-106.
9. Wei X.; Verhaegen M. and V.E. T., *Sensor fault detection and isolation for wind turbines based on subspace identification and Kalman filter techniques.* International Journal of Adaptive Control and Signal Processing, 2010. **24**(8): p. 687-707.
10. Dalsgaard S., Blanke M. and Brath P., *Diagnosis of pitch and load defects*, May 2009, European Patents - EP 2225460-A2 B2.
11. Wei X.; Verhaegen M., *Sensor and actuator fault diagnosis for wind turbine systems by using robust observer and filter.* Wind Energy, 2011. **14**(4): p. 491-516.
12. Zaher A.; McArthur S. J., I.D.G., Patel Y.,, *Online wind turbine fault detection through automated SCADA data analysis.* J. of Wind Energy, 2009. **12**(6): p. 574-593.
13. Nielsen J. S.; Van de Pieterman R. P.; Sørensen J. D., *Analysis of pitch system data for condition monitoring.* Journal of Wind Energy, 2013, DOI 10.1002/we.1586.
14. Yang W.; Tavner P.J.; Crabtree C.J. and W. M., *Cost-effective condition monitoring for wind turbines.* Journal of Industrial Electronics, IEEE Transactions on, (2010). **57**(1): p. 263-271.
15. Jonkman J. M., B.S., Musial W., Scott G.,, *Definition of a 5-MW reference wind turbine for offshore system development*, 2009, National Renewable Energy Laboratory: Houston US.
16. Larsen T. J. and Hansen A. M., *How 2 HAWC2, the user's manual*, 2007, DTU Wind.
17. Larsen T. J. and Hanson T. D., *A method to avoid negative damped low frequent tower vibrations for a floating, pitch controlled wind turbine.* Journal of Physics: Conference Series, 2007. **75**(1): p. 012-073.
18. Jonkman J., L.T., Hansen A., Nygaard T., Maus K., Karimirad M., Gao Z., Moan T. Fylling I., *Offshore Code Comparison Collaboration within IEA Wind Task 23: Phase IV Results Regarding Floating Wind Turbine Modeling; Preprint*, in *European Wind Energy Conference (EWEC)*2010, European Wind Energy Association: Warsaw, Poland, April 20-23.
19. Tavner P. J.; Spinato F.; Bussel, G.J.W. and Koutoulakos E. *Reliability of different wind turbine concepts with relevance to offshore application*. in *European Wind Energy Conference (EWEC)*. 2008. Brussel, Belgium Mar.31-Apr.3: European Wind Energy Association.
20. Ribrant J. and Bertling L., *Survey of failures in wind power systems with focus on Swedish wind power plants during 1997-2005*, in *Power Engineering Society General Meeting, 2007. IEEE*2007, IEEE: Stockholm Denmark, Jun 24-28. p. 1-8.

21. Wilkinson M., H.B., Spinatz F., Gomez E., Bulacio H., Roca J., Tavner P., Feng Y., and Long H., *Methodology and results of the ReliaWind reliability field study*, in *European Wind Energy Conference (EWEC)*2010, European Wind Energy Association: Warsaw, Poland, April 20-23.
22. Hoven V. D., *Power spectrum of horizontal wind speed in the frequency range from 0.0007 to 900 cycles per hour.* Journal of Atmospheric Sciences, 1957. **14**: p. 160-164.
23. Johannessen K., Meling T. S. and Haver S., *Joint distribution for wind and waves in the northern north sea.* International Journal of Offshore and Polar Engineering, 2002. **12**(1).
24. Vincent C. L.; Larsén X. G.; Larsen S. E. and S. P., *Cross-spectra over the sea from observations and mesoscale modelling.* Journal of Boundary-Layer Meteorology, 2012: p. 1-22.
25. Hansen M. O. L, *Aerodynamics of wind turbines* UK: Routledge, 2012.
26. Faltinsen O. M., *Sea loads on ships and offshore structures*. Ocean Technology, ed. Camberidge. Vol. 1. 1993, UK: Cambridge university press.
27. DNV, *DNV-OS-J101 Offshore Standard, Design of Offshore Wind Turbine Structures*, 2004.
28. IEC, *IEC 61400-3*, in *Wind Turbines - Part 3: Design Requirements for Offshore Wind Turbines* 2009, International Electrotechnical Commission: Geneva, Switzerland.
29. Li L.; Zhen G. and Moan T. *Joint Environmental data at five european offshore sites for design of combined wind and wave energy devices*. in *32th International Conference on Ocean, Offshore and Arctic Engineering (OMAE 2013)* 2013, June 9-14. Nantes, France.
30. Brodtkorb P. A.; Johannesson P.; Lindgren G., R.I., Rydén J. and Sjö E. *WAFO–a Matlab toolbox for analysis of random waves and loads*. in *Proceedings of the 10'th (2000) International Offshore and Polar Engineering Conference*. 2000. Seatel, USA.
31. Yang Z.; Blanke M., *A unified approach for controllability analysis of hybrid control systems.* Journal of Nonlinear Analysis: Hybrid Systems 1, 2007: p. 212-222.
32. IEC, *IEC 61400-1: Wind turbines part 1: Design requirements*, in *International Electrotechnical Commission*2005, International Electrotechnical Committee: Geneva, Switzerland.